Discontinuous Galerkin method - a robust solver for compressible flow

Miloslav Feistauer, Jan Česenek and Václav Kučera

Abstract The subject of the paper is the numerical simulation of inviscid and viscous compressible flow in time dependent domains. The motion of the boundary of the domain occupied by the fluid is taken into account with the aid of the ALE (Arbitrary Lagrangian-Eulerian) formulation of the Euler and Navier-Stokes equations describing compressible flow. They are discretized in space by the discontinuous Galerkin (DG) finite element method using piecewise polynomial discontinuous approximations. For the time discretization the BDF method or DG in time is used. Moreover, we use a special treatment of boundary conditions and shock capturing, allowing the solution of flow with a wide range of Mach numbers. As a result we get an efficient and robust numerical process. We show that the method allows to solve numerically the flow with a wide range of Mach numbers and it is applicable to the solution of practically relevant problems of flow induced airfoil vibrations.

1 Introduction

In the numerical solution of compressible flow, we meet several obstacles. It is necessary to resolve accurately shock waves, contact discontinuities and (in viscous flow) boundary layers, wakes and their interaction. These phenomena are connected with the simulation of high speed flow with high Mach numbers. However, it appears that the solution of low Mach number flow is also rather difficult. This is caused by the stiff behaviour of numerical schemes and

Miloslav Feistauer
Department of Numerical Mathematics, Faculty of Mathematics and Physics, Charles University, Sokolovská 83, 18675 Praha 8, e-mail: feist@karlin.mff.cuni.cz

Jan Česenek e-mail: jan.cessa@seznam.cz · Václav Kučera e-mail: kucera@karlin.mff.cuni.cz

acoustic phenomena appearing in low Mach number flows at incompressible limit.

It appears that a suitable numerical method for the solution of compressible flow overcoming these difficulties is the discontinuous Galerkin finite element method (DGFEM). It employs piecewise polynomial approximations without any requirement on the continuity on interfaces between neighbouring elements. The DGFEM was used for the numerical simulation of the compressible Euler equations, for example, by Bassi and Rebay in [1], where the space DG discretization was combined with explicit Runge-Kutta time discretization. In [2] Baumann and Oden describe an *hp* version of the space DG discretization with explicit time stepping to compressible flow. Van der Vegt and van der Ven apply space-time discontinuous Galerkin method to the solution of the Euler equations in [18], where the discrete problem is solved with the aid of a multigrid accelerated pseudo-time-integration.

In a number of practical applications, flow problems in time dependent domains and fluid-structure interaction have to be solved. The flow-induced vibrations of elastic structures may affect negatively the operation and stability of the systems. Therefore, one of the main goals of aeroelasticity is the prediction and alleviation of the aeroelastic instability. This discipline achieved many results, particularly from the engineering point of view (see, e.g. the monographs [3], [8] and [15]).

In our paper we shall describe a numerical method based on the application of the DGFEM for the solution of compressible flow, which is robust with respect to the magnitude of the Mach number and Reynolds number and can be applied to the simulation of flows in time-dependent domains and flow induced airfoil vibrations. The airfoil is considered as a solid flexibly supported body with two degrees of freedom, allowing its vertical and torsional oscillations. The presented examples demonstrate the robustness and applicability of the developed numerical technique. The paper represents an extension and generalization of results from [14] and [17].

2 Description of compressible flow

We shall be concerned with the numerical solution of compressible flow in a bounded domain $\Omega_t \subset \mathbb{R}^2$ depending on time $t \in [0, T]$. Let the boundary of Ω_t consist of three disjoint parts: $\partial\Omega_t = \Gamma_I \cup \Gamma_O \cup \Gamma_{W_t}$, where Γ_I is the inlet, Γ_O is the outlet and Γ_{W_t} denotes impermeable walls that may move in dependence on time.

The system describing compressible flow, consisting of the continuity, Navier-Stokes and energy equation, can be written in the form

$$\frac{\partial \boldsymbol{w}}{\partial t} + \sum_{s=1}^{2} \frac{\partial \boldsymbol{f}_s(\boldsymbol{w})}{\partial x_s} = \sum_{s=1}^{2} \frac{\partial \boldsymbol{R}_s(\boldsymbol{w}, \nabla \boldsymbol{w})}{\partial x_s}, \tag{1}$$

where

$$\begin{aligned}
\boldsymbol{w} &= (w_1,\dots,w_4)^T = (\rho,\rho v_1,\rho v_2,E)^T \in I\!R^4, \qquad (2)\\
\boldsymbol{w} &= \boldsymbol{w}(x,t),\ x\in\Omega_t,\ t\in(0,T),\\
\boldsymbol{f}_i(\boldsymbol{w}) &= (f_{i1},\cdots,f_{i4})^{\mathcal{T}} = (\rho v_i,\rho v_1 v_i+\delta_{1i}\,p,\rho v_2 v_i+\delta_{2i}\,p,(E+p)v_i)^T,\\
\boldsymbol{R}_i(\boldsymbol{w},\nabla\boldsymbol{w}) &= (R_{i1},\dots,R_{i4})^T = \left(0,\tau_{i1}^V,\tau_{i2}^V,\tau_{i1}^V\,v_1+\tau_{i2}^V\,v_2+k\partial\theta/\partial x_i\right)^T,\\
\tau_{ij}^V &= \lambda\,\mathrm{div}\boldsymbol{v}\,\delta_{ij}+2\mu\,d_{ij}(\boldsymbol{v}),\ d_{ij}(\boldsymbol{v}) = \frac{1}{2}\left(\frac{\partial v_i}{\partial x_j}+\frac{\partial v_j}{\partial x_i}\right).
\end{aligned}$$

We use the following notation: ρ – density, p – pressure, E – total energy, $\boldsymbol{v}=(v_1,v_2)$ – velocity, θ – absolute temperature, $\gamma>1$ – Poisson adiabatic constant, $c_v>0$ – specific heat at constant volume, $\mu>0,\lambda=-2\mu/3$ – viscosity coefficients, k – heat conduction. The vector-valued function $\boldsymbol{w}$ is called state vector, the functions $\boldsymbol{f}_i$ are the so-called inviscid fluxes and $\boldsymbol{R}_i$ represent viscous terms.

The above system is completed by the thermodynamical relations

$$p=(\gamma-1)(E-\rho|\boldsymbol{v}|^2/2),\quad \theta=\Big(\frac{E}{\rho}-\frac{1}{2}|\boldsymbol{v}|^2\Big)/c_v. \qquad (3)$$

The resulting system is equipped with the initial condition

$$\boldsymbol{w}(x,0)=\boldsymbol{w}^0(x),\quad x\in\Omega_0, \qquad (4)$$

and the following boundary conditions:

$$\begin{aligned}
&\text{a)}\ \rho|_{\Gamma_I}=\rho_D,\quad \text{b)}\ \boldsymbol{v}|_{\Gamma_I}=\boldsymbol{v}_D=(v_{D1},v_{D2})^{\mathrm{T}}, \qquad (5)\\
&\text{c)}\ \sum_{i,j=1}^{2}\tau_{ij}^V n_i v_j+k\frac{\partial\theta}{\partial n}=0\quad \text{on } \Gamma_I,\\
&\text{d)}\ \boldsymbol{v}|_{\Gamma_{W_t}}=\boldsymbol{z}_D=\text{velocity of a moving wall},\ \text{e)}\ \frac{\partial\theta}{\partial n}|_{\Gamma_{W_t}}=0\ \text{on } \Gamma_{W_t},\\
&\text{f)}\ \sum_{i=1}^{2}\tau_{ij}^V n_i=0,\quad j=1,2,\quad \text{g)}\frac{\partial\theta}{\partial n}=0\ \text{on } \Gamma_O.
\end{aligned}$$

It is easy to see that $\boldsymbol{f}_s(\alpha\boldsymbol{w})=\alpha\ \boldsymbol{f}_s(\boldsymbol{w})$ for $\alpha>0$. This implies that

$$\boldsymbol{f}_s(\boldsymbol{w})=\mathbb{A}_s(\boldsymbol{w})\boldsymbol{w},\quad s=1,2, \qquad (6)$$

where $\mathbb{A}_s(\boldsymbol{w})=D\boldsymbol{f}_s(\boldsymbol{w})/D\boldsymbol{w},\ s=1,2$, are the Jacobi matrices of the mappings $\boldsymbol{f}_s$. The viscous terms $\boldsymbol{R}_s(\boldsymbol{w},\nabla\boldsymbol{w})$ can be expressed in the form

$$\boldsymbol{R}_s(\boldsymbol{w},\nabla\boldsymbol{w})=\sum_{k=1}^{2}\mathbb{K}_{s,k}(\boldsymbol{w})\frac{\partial\boldsymbol{w}}{\partial x_k},\quad s=1,2, \qquad (7)$$

where $\mathbb{K}_{s,k}(\boldsymbol{w}) \in I\!R^{4\times 4}$ are matrices depending on $\boldsymbol{w}$ (cf. [6]).

In order to treat the time dependence of the domain, we use the so-called *arbitrary Lagrangian-Eulerian* ALE technique, see e.g. [16]. We define a reference domain Ω_0 and introduce a regular one-to-one ALE mapping of Ω_0 onto Ω_t:

$$\mathcal{A}_t : \overline{\Omega}_0 \longrightarrow \overline{\Omega}_t, \ \textit{i.e.} \ \boldsymbol{X} \in \overline{\Omega}_0 \longmapsto \boldsymbol{x} = \boldsymbol{x}(\boldsymbol{X}, t) = \mathcal{A}_t(\boldsymbol{X}) \in \overline{\Omega}_t.$$

Here we use the notation $\boldsymbol{X}$ for points in $\overline{\Omega}_0$ and $\boldsymbol{x}$ for points in $\overline{\Omega}_t$.

Further, we define the domain velocity:

$$\tilde{\boldsymbol{z}}(\boldsymbol{X}, t) = \frac{\partial}{\partial t}\mathcal{A}_t(\boldsymbol{X}), \quad t \in [0, T], \ \boldsymbol{X} \in \Omega_0,$$
$$\boldsymbol{z}(\boldsymbol{x}, t) = \tilde{\boldsymbol{z}}(\mathcal{A}^{-1}(\boldsymbol{x}), t), \quad t \in [0, T], \ \boldsymbol{x} \in \Omega_t$$

and the ALE derivative of a function $f = f(\boldsymbol{x}, t)$ defined for $\boldsymbol{x} \in \Omega_t$ and $t \in [0, T]$:

$$\frac{D^A}{Dt} f(\boldsymbol{x}, t) = \frac{\partial \tilde{f}}{\partial t}(\boldsymbol{X}, t), \tag{8}$$

where

$$\tilde{f}(\boldsymbol{X}, t) = f(\mathcal{A}_t(\boldsymbol{X}), t), \ \boldsymbol{X} \in \Omega_0, \ \boldsymbol{x} = \mathcal{A}_t(\boldsymbol{X}).$$

As a direct consequence of the chain rule we get the relation

$$\frac{D^A f}{Dt} = \frac{\partial f}{\partial t} + \operatorname{div}(\boldsymbol{z} f) - f \operatorname{div} \boldsymbol{z}.$$

This leads to the ALE formulation of the Navier-Stokes equations

$$\frac{D^A \boldsymbol{w}}{Dt} + \sum_{s=1}^{2} \frac{\partial \boldsymbol{g}_s(\boldsymbol{w})}{\partial x_s} + \boldsymbol{w} \operatorname{div} \boldsymbol{z} = \sum_{s=1}^{2} \frac{\partial \boldsymbol{R}_s(\boldsymbol{w}, \nabla \boldsymbol{w})}{\partial x_s}, \tag{9}$$

where

$$\boldsymbol{g}_s(\boldsymbol{w}) := \boldsymbol{f}_s(\boldsymbol{w}) - z_s \boldsymbol{w}, \quad s = 1, 2,$$

are the ALE modified inviscid fluxes.

We see that in the ALE formulation of the Navier-Stokes equations the time derivative $\partial \boldsymbol{w}/\partial t$ is replaced by the ALE derivative $D^A \boldsymbol{w}/Dt$, the inviscid fluxes $\boldsymbol{f}_s$ are replaced by the ALE modified inviscid fluxes $\boldsymbol{g}_s$ and a new additional "reaction" term $\boldsymbol{w} \operatorname{div} \boldsymbol{z}$ appears.

3 Discrete flow problem

3.1 Space discretization by the discontinuous Galerkin method

For the space semidiscretization we use the discontinuous Galerkin finite element method (DGFEM). We construct a polygonal approximation Ω_{ht} of the domain Ω_t. By $\mathcal{T}_{ht}$ we denote a partition of the closure $\overline{\Omega}_{ht}$ of the domain Ω_{ht} into a finite number of closed triangles K with mutually disjoint interiors such that $\overline{\Omega}_{ht} = \bigcup_{K\in\mathcal{T}_{ht}} K$.

By $\mathcal{F}_{ht}$ we denote the system of all faces of all elements $K \in \mathcal{T}_{ht}$. Further, we introduce the set of boundary faces $\mathcal{F}_{ht}^B = \{\Gamma \in \mathcal{F}_{ht};\ \Gamma \subset \partial\Omega_{ht}\}$, the set of "Dirichlet" boundary faces $\mathcal{F}_{ht}^D = \{\Gamma \in \mathcal{F}_{ht}^B$; a Dirichlet condition is prescribed on $\Gamma\}$ and the set of inner faces $\mathcal{F}_{ht}^I = \mathcal{F}_{ht} \setminus \mathcal{F}_{ht}^B$. Each $\Gamma \in \mathcal{F}_{ht}$ is associated with a unit normal vector $\boldsymbol{n}_\Gamma$ to Γ. For $\Gamma \in \mathcal{F}_{ht}^B$ the normal $\boldsymbol{n}_\Gamma$ has the same orientation as the outer normal to $\partial\Omega_{ht}$. We set $d(\Gamma)$ = length of $\Gamma \in \mathcal{F}_{ht}$ and $h_K =$ diameter of $K \in \mathcal{T}_{ht}$.

For each $\Gamma \in \mathcal{F}_{ht}^I$ there exist two neighbouring elements $K_\Gamma^{(L)}, K_\Gamma^{(R)} \in \mathcal{T}_h$ such that $\Gamma \subset \partial K_\Gamma^{(R)} \cap \partial K_\Gamma^{(L)}$. We use the convention that $K_\Gamma^{(R)}$ lies in the direction of $\boldsymbol{n}_\Gamma$ and $K_\Gamma^{(L)}$ lies in the opposite direction to $\boldsymbol{n}_\Gamma$. If $\Gamma \in \mathcal{F}_{ht}^B$, then the element adjacent to Γ will be denoted by $K_\Gamma^{(L)}$.

The approximate solution will be sought in the space of piecewise polynomial functions

$$\boldsymbol{S}_{ht} = [S_{ht}]^4, \quad \text{with} \quad S_{ht} = \{v; v|_K \in P_r(K)\ \forall\, K \in \mathcal{T}_{ht}\}, \tag{10}$$

where $r > 0$ is an integer and $P_r(K)$ denotes the space of all polynomials on K of degree $\le r$. A function $\boldsymbol{\varphi} \in \boldsymbol{S}_{ht}$ is, in general, discontinuous on interfaces $\Gamma \in \mathcal{F}_{ht}^I$. By $\boldsymbol{\varphi}_\Gamma^{(L)}$ and $\boldsymbol{\varphi}_\Gamma^{(R)}$ we denote the values of $\boldsymbol{\varphi}$ on Γ considered from the interior and the exterior of $K_\Gamma^{(L)}$, respectively, and set $\langle\boldsymbol{\varphi}\rangle_\Gamma = (\boldsymbol{\varphi}_\Gamma^{(L)} + \boldsymbol{\varphi}_\Gamma^{(R)})/2$, $[\boldsymbol{\varphi}]_\Gamma = \boldsymbol{\varphi}_\Gamma^{(L)} - \boldsymbol{\varphi}_\Gamma^{(R)}$.

The discrete problem is derived in the following way: We multiply system (9) by a test function $\boldsymbol{\varphi}_h \in \boldsymbol{S}_{ht}$, integrate over $K \in \mathcal{T}_{ht}$, apply Green's theorem, sum over all elements $K \in \mathcal{T}_{ht}$, use the concept of the numerical flux and introduce suitable terms mutually vanishing for a regular exact solution and linearize the resulting forms on the basis of properties (6) and (7) of the functions $\boldsymbol{f}_s$ and $\boldsymbol{R}_s$ (see, e.g. [13]). In this way we get the following forms (followed by the explanation of symbols appearing in their definitions):

$$\hat{a}_h(\overline{\boldsymbol{w}}_h, \boldsymbol{w}_h, \boldsymbol{\varphi}_h, t) = \sum_{K\in\mathcal{T}_{ht}} \int_K \sum_{s=1}^{2}\sum_{k=1}^{2} \mathbb{K}_{s,k}(\overline{\boldsymbol{w}}_h)\ \frac{\partial \boldsymbol{w}_h}{\partial x_k}\cdot\frac{\partial \boldsymbol{\varphi}_h}{\partial x_s}\ \mathrm{d}\boldsymbol{x} \tag{11}$$

$$- \sum_{\Gamma\in\mathcal{F}_{ht}^I} \int_\Gamma \sum_{s=1}^{2} \left\langle \sum_{k=1}^{2} \mathbb{K}_{s,k}(\overline{\boldsymbol{w}}_h)\frac{\partial \boldsymbol{w}_h}{\partial x_k} \right\rangle (\boldsymbol{n}_\Gamma)_s \cdot [\boldsymbol{\varphi}_h]\ \mathrm{d}S$$

$$- \sum_{\Gamma\in\mathcal{F}_{ht}^D} \int_\Gamma \sum_{s=1}^{2}\sum_{k=1}^{2} \mathbb{K}_{s,k}(\overline{\boldsymbol{w}}_h)\frac{\partial \boldsymbol{w}_h}{\partial x_k}(\boldsymbol{n}_\Gamma)_s \cdot \boldsymbol{\varphi}_h\ \mathrm{d}S$$

$$- \Theta \sum_{\Gamma\in\mathcal{F}_{ht}^I} \int_\Gamma \sum_{s=1}^{2} \left\langle \sum_{k=1}^{2} \mathbb{K}_{k,s}^T(\overline{\boldsymbol{w}}_h)\frac{\partial \boldsymbol{\varphi}_h}{\partial x_k} \right\rangle (\boldsymbol{n}_\Gamma)_s \cdot [\boldsymbol{w}_h]\ \mathrm{d}S$$

$$- \Theta \sum_{\Gamma\in\mathcal{F}_{ht}^D} \int_\Gamma \sum_{s=1}^{2}\sum_{k=1}^{2} \mathbb{K}_{k,s}^T(\overline{\boldsymbol{w}}_h)\frac{\partial \boldsymbol{\varphi}_h}{\partial x_k}(\boldsymbol{n}_\Gamma)_s \cdot \boldsymbol{w}_h\ \mathrm{d}S,$$

$$d_h(\boldsymbol{w}_h, \boldsymbol{\varphi}_h, t) = \sum_{K\in\mathcal{T}_{ht}} \int_K (\boldsymbol{w}_h\cdot\boldsymbol{\varphi}_h)\,\mathrm{div}\boldsymbol{z}\ \mathrm{d}x, \tag{12}$$

$$J_h(\boldsymbol{w}_h, \boldsymbol{\varphi}_h, t) = \sum_{\Gamma\in\mathcal{F}_{ht}^I} \int_\Gamma \sigma[\boldsymbol{w}_h]\cdot[\boldsymbol{\varphi}_h]\ \mathrm{d}S + \sum_{\Gamma\in\mathcal{F}_{ht}^D} \int_\Gamma \sigma \boldsymbol{w}_h\cdot\boldsymbol{\varphi}_h\ \mathrm{d}S, \tag{13}$$

$$\ell_h(\boldsymbol{w}_h, \boldsymbol{\varphi}_h, t) = \sum_{\Gamma\in\mathcal{F}_{ht}^D} \int_\Gamma \sum_{s=1}^{2} \sigma \boldsymbol{w}_B\cdot\boldsymbol{\varphi}_h\ \mathrm{d}S \tag{14}$$

$$- \Theta \sum_{\Gamma\in\mathcal{F}_{ht}^D} \int_\Gamma \sum_{s=1}^{2}\sum_{k=1}^{2} \mathbb{K}_{k,s}^T(\overline{\boldsymbol{w}}_h)\frac{\partial \boldsymbol{\varphi}_h}{\partial x_k}(\boldsymbol{n}_\Gamma)_s \cdot \boldsymbol{w}_B\ \mathrm{d}S,$$

$$\hat{b}_h(\overline{\boldsymbol{w}}_h, \boldsymbol{w}_h, \boldsymbol{\varphi}_h, t) = \tag{15}$$

$$- \sum_{K\in\mathcal{T}_{ht_{k+1}}} \int_K \sum_{s=1}^{2} (\mathbb{A}_s(\overline{\boldsymbol{w}}_h(x)) - z_s(x))\mathbb{I})\boldsymbol{w}_h(x))\cdot\frac{\partial \boldsymbol{\varphi}_h(x)}{\partial x_s}dx$$

$$+ \sum_{\Gamma\in\mathcal{F}_{ht}^I} \int_\Gamma \left(\mathbb{P}_g^+\left(\langle\overline{\boldsymbol{w}}_h\rangle_\Gamma, \boldsymbol{n}_\Gamma\right)\boldsymbol{w}_h^{(L)} + \mathbb{P}_g^-\left(\langle\overline{\boldsymbol{w}}_h\rangle_\Gamma, \boldsymbol{n}_\Gamma\right)\boldsymbol{w}_h^{(R)}\right)\cdot[\boldsymbol{\varphi}_h]\ \mathrm{d}S$$

$$+ \sum_{\Gamma\in\mathcal{F}_{ht}^B} \int_\Gamma \left(\mathbb{P}_g^+\left(\langle\overline{\boldsymbol{w}}_h\rangle_\Gamma, \boldsymbol{n}_\Gamma\right)\boldsymbol{w}_h^{(L)} + \mathbb{P}_g^-\left(\langle\overline{\boldsymbol{w}}_h\rangle_\Gamma, \boldsymbol{n}_\Gamma\right)\overline{\boldsymbol{w}}_h^{(R)}\right)\cdot\boldsymbol{\varphi}_h\ \mathrm{d}S,$$

We set $\Theta = 1$ or $\Theta = 0$ or $\Theta = -1$ and get the so-called symmetric version (SIPG) or incomplete version (IIPG) or nonsymmetric version (NIPG), respectively, of the discretization of viscous terms.

The symbols $\mathbb{P}^+(\boldsymbol{w}, \boldsymbol{n})$ and $\mathbb{P}^-(\boldsymbol{w}, \boldsymbol{n})$ denote the positive and negative part of the matrix $\mathbb{P}(\boldsymbol{w}, \boldsymbol{n}) = \sum_{s=1}^{2}(\mathbb{A}_s(\boldsymbol{w}) - z_s\mathbb{I})n_s$ defined in the following way. By [12], this matrix is diagonalizable. It means that there exists a nonsingular matrix $\mathbb{T} = \mathbb{T}(\boldsymbol{w}, \boldsymbol{n})$ such that

$$\mathbb{P}_g = \mathbb{T}\mathbb{\Lambda}\mathbb{T}^{-1}, \quad \mathbb{\Lambda} = \mathrm{diag}(\lambda_1, \ldots, \lambda_4), \tag{16}$$

where $\lambda_i = \lambda_i(\boldsymbol{w}, \boldsymbol{n})$ are eigenvalues of the matrix $\mathbb{P}_g$. Now we define the "positive" and "negative" parts of the matrix $\mathbb{P}_g$ by

$$\mathbb{P}^{\pm} = \mathbb{T}\mathbb{\Lambda}^{\pm}\mathbb{T}^{-1}, \quad \mathbb{\Lambda}^{\pm} = \mathrm{diag}(\lambda_1^{\pm}, \ldots, \lambda_4^{\pm}), \tag{17}$$

where $\lambda^+ = \max(\lambda, 0),\ \lambda^- = \min(\lambda, 0)$. Using the above concepts, we introduce the modified Vijayasundaram numerical flux (cf. [19] or [12]) as

$$\boldsymbol{H}(\boldsymbol{w}_L, \boldsymbol{w}_R, \boldsymbol{n}) = \mathbb{P}^+\Big(\frac{\boldsymbol{w}_L + \boldsymbol{w}_R}{2}, \boldsymbol{n}\Big)\boldsymbol{w}_L + \mathbb{P}^-\Big(\frac{\boldsymbol{w}_L + \boldsymbol{w}_R}{2}, \boldsymbol{n}\Big)\boldsymbol{w}_R, \tag{18}$$

which is used in the definition of the convective form (15).

In (13), $\sigma|_\Gamma = C_W \mu / d(\Gamma)$ and $C_W > 0$ is a sufficiently large constant. The boundary state $\boldsymbol{w}_B$ is defined on the basis of the Dirichlet boundary conditions (5), a), b), d) and extrapolation:

$$\boldsymbol{w}_B = (\rho_D, \rho_D v_{D1}, \rho_D v_{D2}, c_v \rho_D \theta_\Gamma^{(L)} + \frac{1}{2}\rho_D |\boldsymbol{v}_D|^2) \quad \text{on } \Gamma_I, \tag{19}$$

$$\boldsymbol{w}_B = \boldsymbol{w}_\Gamma^{(L)} \quad \text{on } \Gamma_O, \tag{20}$$

$$\boldsymbol{w}_B = (\rho_\Gamma^{(L)}, \rho_\Gamma^{(L)} z_{D1}, \rho_\Gamma^{(L)} z_{D2}, c_v \rho_\Gamma^{(L)} \theta_\Gamma^{(L)} + \frac{1}{2}\rho_\Gamma^{(L)} |\boldsymbol{z}_D|^2) \quad \text{on } \Gamma_{W_t}. \tag{21}$$

For $\Gamma \in \mathcal{F}_{ht}^B$ we set $\langle \overline{\boldsymbol{w}}_h \rangle_\Gamma = (\overline{\boldsymbol{w}}_\Gamma^{(L)} + \overline{\boldsymbol{w}}_\Gamma^{(R)})/2$ and the boundary state $\overline{\boldsymbol{w}}_\Gamma^{(R)}$ is defined with the aid of the solution of the 1D linearized initial-boundary Riemann problem as in [11].

In order to avoid spurious oscillations in the approximate solution in the vicinity of discontinuities or steep gradients, we apply artificial viscosity forms. They are based on the discontinuity indicator

$$g_t(K) = \int_{\partial K} [\overline{\rho}_h]^2 \ \mathrm{d}S \big/ (h_K |K|^{3/4}), \quad K \in \mathcal{T}_{ht}, \tag{22}$$

introduced in [7]. By $[\overline{\rho}_h]$ we denote the jump of the function $\overline{\rho}_h$ on the boundary ∂K and $|K|$ denotes the area of the element K. Then we define the discrete discontinuity indicator $G_t(K) = 0$ if $g_t(K) < 1$, $G_t(K) = 1$ if $g_t(K) \geq 1$, and the artificial viscosity forms (see [14])

$$\hat{\beta}_h(\overline{\boldsymbol{w}}_h, \boldsymbol{w}_h, \boldsymbol{\varphi}_h, t) = \nu_1 \sum_{K \in \mathcal{T}_{ht}} h_K G_t(K) \int_K \nabla \boldsymbol{w}_h \cdot \nabla \boldsymbol{\varphi}_h \ \mathrm{d}\boldsymbol{x}, \tag{23}$$

$$\hat{J}_h(\overline{\boldsymbol{w}}_h, \boldsymbol{w}_h, \boldsymbol{\varphi}_h, t) = \nu_2 \sum_{\Gamma \in \mathcal{F}_h^I} \frac{1}{2}\big(G_t(K_\Gamma^{(L)}) + G_t(K_\Gamma^{(R)})\big) \int_\Gamma [\boldsymbol{w}_h] \cdot [\boldsymbol{\varphi}_h] \ \mathrm{d}S,$$

with parameters ν_1, $\nu_2 = O(1)$.

In order to increase the quality of the numerical approximations, in [4], isoparametric elements were used.

3.2 Time discretization by the BDF method

Let us construct a partition $0 = t_0 < t_1 < t_2 \ldots$ of the time interval $[0, T]$ and define the time step $\tau_n = t_n - t_{n-1}$. We use the approximations $\boldsymbol{w}_h(t_n) \approx \boldsymbol{w}_h^n \in \boldsymbol{S}_{ht_n}$, $\boldsymbol{z}(t_n) \approx \boldsymbol{z}^n$, $n = 0, 1, \ldots$. Let us assume that $\boldsymbol{w}_h^n$, $n = 0, \ldots, m-1$, are already known. Then we introduce the functions $\hat{\boldsymbol{w}}_h^n = \boldsymbol{w}_h^n \circ \mathcal{A}_{t_n} \circ \mathcal{A}_{t_m}^{-1}$ for $n = m-1, m-2, \ldots$, which are defined in the domain Ω_{ht_m}. The ALE derivative at time t_m is approximated by the backward finite difference formula (BDF) of order q:

$$\frac{D^{\mathcal{A}}\boldsymbol{w}_h}{Dt}(t_m) \approx \frac{D^{\mathcal{A}}_{appr}\boldsymbol{w}_h}{Dt}(t_m) = \alpha_0 \boldsymbol{w}_h^m + \sum_{l=1}^{q} \alpha_l \hat{\boldsymbol{w}}_h^{m-l},$$

with coefficients α_l, $l = 0, ..., q$, depending on τ_{m-l}, $l = 0, ..., q-1$. In the beginning of the computation, when $m < q$, we approximate the ALE derivative by formulas of the lower order $q := m$. In nonlinear terms we use the extrapolation for the computation of the state $\overline{\boldsymbol{w}}_h^m$:

$$\overline{\boldsymbol{w}}_h^m = \sum_{l=1}^{q} \beta_l \hat{\boldsymbol{w}}_h^{m-l}, \tag{24}$$

where β_l, $l = 1, ..., q$, depend on τ_{m-l}, $l = 0, ..., q-1$. If $m < q$, then we apply extrapolation of order m. Namely, for $q = 1$ we have

$$\frac{D^{\mathcal{A}}_{appr}\boldsymbol{w}_h}{Dt}(t_m) = \frac{\boldsymbol{w}_h^m - \hat{\boldsymbol{w}}_h^{m-1}}{\tau_m} \tag{25}$$

and

$$\overline{\boldsymbol{w}}_h^m = \hat{\boldsymbol{w}}_h^{m-1}. \tag{26}$$

If $q = 2$, then

$$\begin{aligned} &\frac{D^{\mathcal{A}}_{appr}\boldsymbol{w}_h}{Dt}(t_m) \\ &= \frac{2\tau_m + \tau_{m-1}}{\tau_m(\tau_m + \tau_{m-1})}\boldsymbol{w}_h^{m+1} - \frac{\tau_m + \tau_{m-1}}{\tau_m \tau_{m-1}}\hat{\boldsymbol{w}}_h^m + \frac{\tau_m}{\tau_{m-1}(\tau_m + \tau_{m-1})}\hat{\boldsymbol{w}}_h^{m-1} \end{aligned} \tag{27}$$

and

$$\overline{\boldsymbol{w}}_h^m = \frac{\tau_m + \tau_{m-1}}{\tau_{m-1}}\hat{\boldsymbol{w}}_h^m - \frac{\tau_m}{\tau_{m-1}}\hat{\boldsymbol{w}}_h^{m-1}. \tag{28}$$

By the symbol $(\cdot, \cdot)_{t_m}$ we shall denote the scalar product in $L^2(\Omega_{ht_m})$, i.e.

$$(\boldsymbol{w}_h, \boldsymbol{\varphi}_h)_{t_m} = \int_{\Omega_{ht_m}} \boldsymbol{w}_h \cdot \boldsymbol{\varphi}_h \, dx. \tag{29}$$

The resulting *BDF-DG scheme* has the following form: For each $m = 1, 2, \ldots$ we seek $\boldsymbol{w}_h^m \in \boldsymbol{S}_{ht_m}$ such that

$$\left(\frac{D^{\mathcal{A}}_{appr}\boldsymbol{w}_h}{Dt}(t_m), \boldsymbol{\varphi}_h\right)_{t_m} + \hat{b}_h(\overline{\boldsymbol{w}}_h^m, \boldsymbol{w}_h^m, \boldsymbol{\varphi}_h, t_m) + \hat{a}_h(\overline{\boldsymbol{w}}_h^m, \boldsymbol{w}_h^m, \boldsymbol{\varphi}_h, t_m) \quad (30)$$
$$+ J_h(\boldsymbol{w}_h^m, \boldsymbol{\varphi}_h, t_m) + d_h(\boldsymbol{w}_h^m, \boldsymbol{\varphi}_h, t_m) + \hat{\beta}_h(\overline{\boldsymbol{w}}_h^m, \boldsymbol{w}_h^m, \boldsymbol{\varphi}_h, t_m)$$
$$+ \hat{J}_h(\overline{\boldsymbol{w}}_h^m, \boldsymbol{w}_h^m, \boldsymbol{\varphi}_h, t_m) = \ell(\overline{\boldsymbol{w}}_B^m, \boldsymbol{\varphi}_h, t_m), \quad \forall \boldsymbol{\varphi}_h \in \boldsymbol{S}_{ht_m}.$$

3.3 Space-time discontinuous Galerkin method

We again consider a partition $0 = t_0 < t_1 < \ldots < t_M = T$ of the time interval $[0, T]$ and denote $I_m = (t_{m-1}, t_m)$, $\overline{I}_m = [t_{m-1}, t_m]$, $\tau_m = t_m - t_{m-1}$, for $m = 1, \ldots, M$. We define the space $\mathbf{S}_{h,\tau}^{r,q} = (S_{h,\tau}^{r,q})^4$, where

$$S_{h,\tau}^{r,q} = \left\{ \phi \,;\, \phi|_{I_m} = \sum_{i=0}^{q} \zeta_i \phi_i, \text{ where } \phi_i \in S_{ht},\ \zeta_i \in P^q(I_m) \right\}$$

with integers $r, q \geq 1$, $P^q(I_m)$ denoting the space of all polynomials in t on I_m of degree $\leq q$ and the space S_{ht} defined in (10). For $\boldsymbol{\varphi} \in \mathbf{S}_{h,\tau}^{r,q}$ we introduce the following notation:

$$\boldsymbol{\varphi}_m^{\pm} = \boldsymbol{\varphi}(t_m^{\pm}) = \lim_{t \to t_{m\pm}} \boldsymbol{\varphi}(t), \quad \{\boldsymbol{\varphi}\}_m = \boldsymbol{\varphi}_m^{+} - \boldsymbol{\varphi}_m^{-}. \quad (31)$$

The derivation of the discrete problem can be carried out similarly as above. The difference is now that time t is considered continuous, test functions $\boldsymbol{\varphi}_{h\tau} \in \mathbf{S}_{h,\tau}^{r,q}$ are used and also the the integration over I_m is applied. In order to bind the solution on intervals I_{m-1} and I_m, we augment the resulting identity by the penalty expression $\left(\{\boldsymbol{w}_{h\tau}\}_{m-1}, \boldsymbol{\varphi}_{h\tau}(t_{m-1}^{+})\right)_{t_{m-1}}$. The initial state $\boldsymbol{w}_{h\tau}(0+) \in S_{h0}^p$ is defined as the $L^2(\Omega_{h0})$-projection of $\boldsymbol{w}^0$ on S_{h0}^p, i.e.

$$(\boldsymbol{w}_{h\tau}(0+), \boldsymbol{\varphi}_h)_{t_0} = \left(\boldsymbol{w}^0, \boldsymbol{\varphi}_h\right)_{t_0} \quad \forall \boldsymbol{\varphi}_h \in \mathbf{S}_{h0}^p. \quad (32)$$

Similarly as in Section 3.2 we introduce the linearization with aid of the extrapolation $\overline{\boldsymbol{w}}_{h\tau}(t) := \boldsymbol{w}_{h\tau}(t_{m-1}^{-})$ for $t \in I_m$.

Now the *space-time DG (STDG) approximate solution* is defined as a function $\boldsymbol{w}_{h\tau} \in \mathcal{S}_{h,\tau}^{r,q}$ satisfying (32) and the following relation for $m = 1, ..., M$:

$$\int_{I_m} \left(\left(\frac{D^{\mathcal{A}} \boldsymbol{w}_{h\tau}}{Dt}(t), \boldsymbol{\varphi}_{h\tau} \right)_t + \hat{a}_h(\overline{\boldsymbol{w}}_{h\tau}, \boldsymbol{w}_{h\tau}, \boldsymbol{\varphi}_{h\tau}, t) \right) \, \mathrm{d}t \tag{33}$$
$$+ \int_{I_m} \left(\hat{b}_h(\overline{\boldsymbol{w}}_{h\tau}, \boldsymbol{w}_{h\tau}, \boldsymbol{\varphi}_{h\tau}, t) + \int_{I_m} J_h(\boldsymbol{w}_{h\tau}, \boldsymbol{\varphi}_{h\tau}, t) \right) \, \mathrm{d}t$$
$$+ \int_{I_m} \left(\hat{\beta}_h(\overline{\boldsymbol{w}}_{h\tau}, \boldsymbol{w}_{h\tau}, \boldsymbol{\varphi}_{h\tau}, t) + \hat{J}_h(\overline{\boldsymbol{w}}_{h\tau}, \boldsymbol{w}_{h\tau}, \boldsymbol{\varphi}_{h\tau}, t) \right) \, \mathrm{d}t$$
$$+ (\{\boldsymbol{w}_{h\tau}\}_{m-1}, \boldsymbol{\varphi}_{h\tau}(t_{m-1}+)) = \int_{I_m} \ell_h(\boldsymbol{w}_{hD}, \boldsymbol{\varphi}_{h\tau}, t) \, \mathrm{d}t, \quad \forall \boldsymbol{\varphi}_{h\tau} \in \mathbf{S}_{h,\tau}^{r,q}.$$

Remark 1. In practical computations, integrals appearing in the definitions of the forms $\hat{a}_h$, $\hat{b}_h$, d_h, J_h, $\hat{J}_h$ and $\hat{\beta}_h$ and also the time integrals are evaluated with the aid of quadrature formulas.

The linear algebraic systems equivalent to (30) and (33) are solved either by the direct solver UMFPACK ([5]) or by the GMRES method with block diagonal preconditioning.

The developed numerical schemes can also be used for the numerical solution of inviscid flow described by the Euler equations. This means that we consider $\mu = \lambda = k = 0$.

4 Numerical experiments

In this section, we shall present results of numerical examples proving that the worked out method allows the numerical solution with very low Mach number flow as well as high-speed flow. Moreover, the application to fluid-structure interaction will be demonstrated.

4.1 Inviscid stationary flow with low Mach number

First we present numerical experiments carried out in [14] in the case of inviscid low Mach number flow at the incompressible limit. We consider flow past a negatively oriented Joukowski profile given by parameters $\Delta = 0.07, a = 0.5, h = 0.05$ (under the notation from [10], Section 2.2.68) with zero angle of attack. The flow is irrotational and homoentropic, because the far-field quantities are constant. The complex function method from [10], allowed us to obtain the exact solution of incompressible inviscid irrotational flow. The velocity circulation is chosen in such a way that the Kutta–Joukowski trailing condition is satisfied.

Compressible inviscid flow past the profile with far-field Mach number $M_\infty = 0.0001$ was computed by the developed scheme (30), using the first-order BDF time discretization. The steady state solution was obtained via

time stabilization for "$t \to \infty$". This means that the numerical scheme was used as an iterative process for "$k \to \infty$". This process was stopped, when the approximation of the time derivative satisfied the condition

$$\left\| \frac{\boldsymbol{w}_h^m - \boldsymbol{w}_h^{m-1}}{\tau_m} \right\|_{L^\infty(\Omega)} < 10^{-8}. \tag{34}$$

Figure 1 shows a detail near the profile of the velocity isolines for the exact solution of incompressible flow and for the approximate solution of compressible flow. In Figure 2, pressure isolines of incompressible and compressible flow are plotted. Further, in Figures 3 and 4, the velocity distribution and pressure coefficient distribution, respectively, past the profile is plotted in the direction from the leading edge to the trailing edge ($\circ\circ\circ$ – exact solution of incompressible flow, —— – approximate solution of compressible flow). The pressure coefficient was defined as $10^7 \cdot (p - p_\infty)$, where p_∞ denotes the far field pressure. The maximum density variation is $1.04 \cdot 10^{-8}$, which means that the computed flow field is practically incompressible.

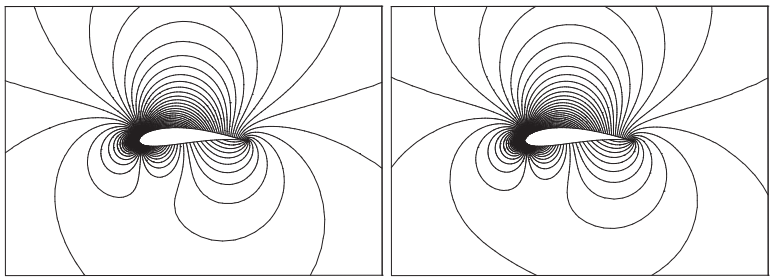

Fig. 1 Velocity isolines for the exact solution of incompressible flow (left) and approximate solution of compressible flow (right)

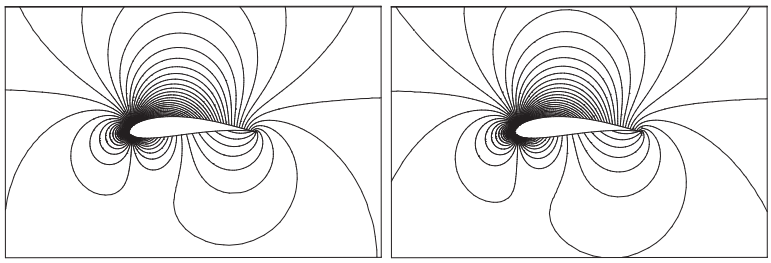

Fig. 2 Pressure isolines for the exact solution of incompressible flow (left) and approximate solution of compressible flow (right)

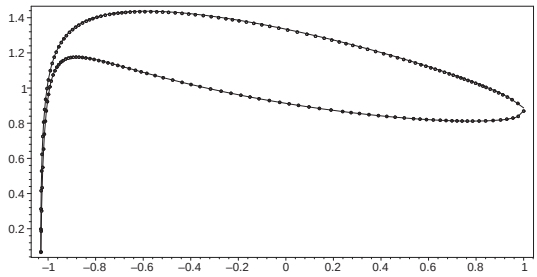

Fig. 3 Flow past a Joukowski profile, velocity distribution along the profile: ○ ○ ○ – exact solution of incompressible flow, —— – approximate solution of compressible flow

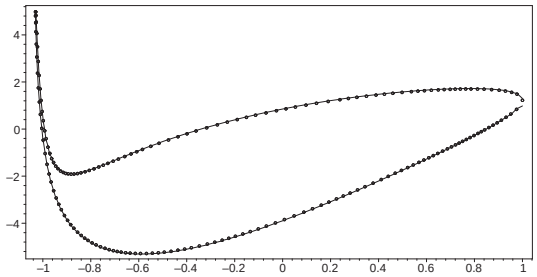

Fig. 4 Flow past a Joukowski profile, pressure distribution along the profile: ○ ○ ○ – exact solution of incompressible flow, —— – approximate solution of compressible flow

4.2 Flow induced airfoil vibrations

The second example is concerned with the simulation of vibrations of an elastically supported NACA 0012 airfoil, induced by compressible viscous flow. The airfoil has two degrees of freedom: the vertical displacement H (positively oriented downwards) and the angle of rotation around an elastic axis α (positively oriented clockwise), cf. Figure 5. The motion of the airfoil is described by the system of nonlinear ordinary differential equations for the unknowns H and α:

$$\begin{aligned} m\ddot{H} + k_{HH}H + S_\alpha\,\ddot{\alpha}\,\cos\alpha - S_\alpha\dot{\alpha}^2\sin\alpha + d_{HH}\dot{H} &= -\mathcal{L}(t), \\ S_\alpha\ddot{H}\cos\alpha + I_\alpha\ddot{\alpha} + k_{\alpha\alpha}\alpha + d_{\alpha\alpha}\dot{\alpha} &= \mathcal{M}(t). \end{aligned} \tag{35}$$

The dot and two dots denote the first- and second-order time derivative, respectively. We use the following notation: $\mathcal{L}(t)$ – aerodynamic lift force (upwards positive), $\mathcal{M}(t)$ – aerodynamic torsional moment (clockwise positive), m - mass of the airfoil, S_α – static moment around the elastic axis EO, I_α – inertia moment around the elastic axis EO, k_{HH} – bending stiffness, $k_{\alpha\alpha}$

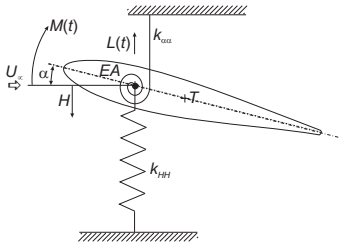

Fig. 5 Elastically supported airfoil with two degrees of freedom.

– torsional stiffness, d_{HH} – structural damping in bending, $d_{\alpha\alpha}$ – structural damping in torsion, c - length of the chord of the airfoil, l – airfoil depth.

System (35) is equipped with the initial conditions prescribing the values $H(0), \alpha(0),\ \dot{H}(0), \dot{\alpha}(0)$. It is transformed to a first-order ODE system and solved numerically by the fourth-order Runge-Kutta method. For the derivation of equations (35), see [17]. The aerodynamic lift force $\mathcal{L}$ acting in the vertical direction and the torsional moment $\mathcal{M}$ are defined by

$$\mathcal{L} = -\,l \int_{\Gamma_{Wt}} \sum_{j=1}^{2} \tau_{2j} n_j dS, \quad \mathcal{M} = \, l \int_{\Gamma_{Wt}} \sum_{i,j=1}^{2} \tau_{ij} n_j r_i^{\mathrm{ort}} dS, \tag{36}$$

where

$$\begin{aligned} &\tau_{ij} = (-p + \lambda \operatorname{div} \boldsymbol{v})\delta_{ij} + \mu\Big(\frac{\partial u_i}{\partial x_j} + \frac{\partial u_j}{\partial x_i}\Big), \\ &r_1^{\mathrm{ort}} = -(x_2 - x_{EO2}),\ r_2^{\mathrm{ort}} = x_1 - x_{EO1}. \end{aligned} \tag{37}$$

By τ_{ij} we denote the components of the stress tensor, δ_{ij} denotes the Kronecker symbol, $\boldsymbol{n} = (n_1, n_2)$ is the unit outer normal to $\partial\Omega_t$ on Γ_{Wt} (pointing into the airfoil) and $x_{EO} = (x_{EO1}, x_{EO2})$ is the position of the elastic axis (lying in the interior of the airfoil). Relations (36) and (37) define the coupling of the fluid dynamical model with the structural model.

In the solution of the complete coupled fluid-structure interaction problem we apply the following algorithm:

1) Assume that the approximate solution of the discrete flow problem at time levels t_{m-2} and t_{m-1} is known and the force $\mathcal{L}$ and torsional moment $\mathcal{M}$ are computed from (36).

2) Extrapolate $\mathcal{L}$ and $\mathcal{M}$ on the time interval $[t_{m-1}, t_m]$.

3) Compute the displacement H and angle α at time t_m as the solution of system (35).

4) Determine the position of the airfoil at time t_m, the domain Ω_{t_m}, the ALE mapping and the domain velocity at time t_m.

5) Solve the discrete system at time t_m.

6) Compute $\mathcal{L}$ and $\mathcal{M}$ at time t_{k+1} and interpolate $\mathcal{L}$ and $\mathcal{M}$ on $[t_{m-1}, t_m]$.

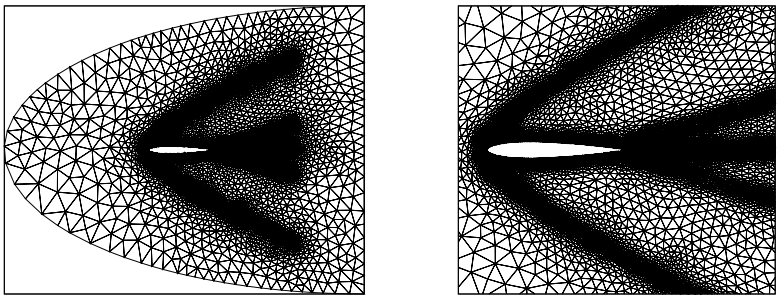

Fig. 6 Triangulation with 42821 elements and its detail near the airfoil.

7) Is higher accuracy needed? YES: go to 3); NO: $m := m + 1$, go to 2).

If in step 7) one goes to 2), the so-called loose (weak) coupling is applied. In our numerical experiments the stronger coupling was applied with $4 - 5$ loops for obtaining the difference between two approximations of H and α less than 10^{-5}. The ALE mapping and the domain velocity are computed in the same way as in [9].

The developed methods allow the numerical simulation of airfoil vibrations induced by low Mach number flows as well as high-speed transonic and hypersonic flows with large Reynolds numbers. It appears that in the method combining the DG space discretization with the BDF time discretization instabilities may appear for flows with far-field Mach numbers higher than 1.5. This is not the case of the space-time DG method, which is very robust and stable for a large range of Mach and Reynolds numbers. Here we present the results of the simulation of airfoil vibrations induced by the flow with far-field Mach number $M_\infty = 3$ and Reynolds numbers 10^4 and 10^5. Here we present the results of computations carried out with the following data: $m = 0.086622$ kg, $S_\alpha = -0.000779673$ kg m, $I_\alpha = 0.000487291$ kg m^2, $k_{HH} = 105109$ N/m, $k_{\alpha\alpha} = 3696.682$ Nm/rad, $l = 0.05$ m, $c = 0.3$ m, $\mu = 1.8375 \cdot 10^{-5}$ kg m^{-1} s^{-1}, far-field density $\rho = 1.225$ kg m^{-3}, $H(0) = 0.02$ m, $\alpha(0) = 6$ degrees, $\dot{H}(0) = 0, \dot{\alpha} = 0$. Structural damping is neglected. The elastic axis is placed on the airfoil chord at 40% distance from the leading edge.

The solution of the flow problem was realized by the space-time DG method with quadratic elements in space ($r = 2$) and linear elements in time ($q = 1$) and SIPG version of the viscous terms discretization. The parameter $C_W = 500$ in the interior part of the penalty form J_h was used, whereas in the boundary penalty $C_W = 5000$. The constants in the artificial viscosity forms were chosen $\nu_1 = \nu_2 = 0.1$.

The computational process started at time $t = -\delta < 0$ by the solution of the flow, keeping the airfoil in a fixed position given by the prescribed initial translation H and the angle of attack α. Then, at time $t = 0$ the airfoil

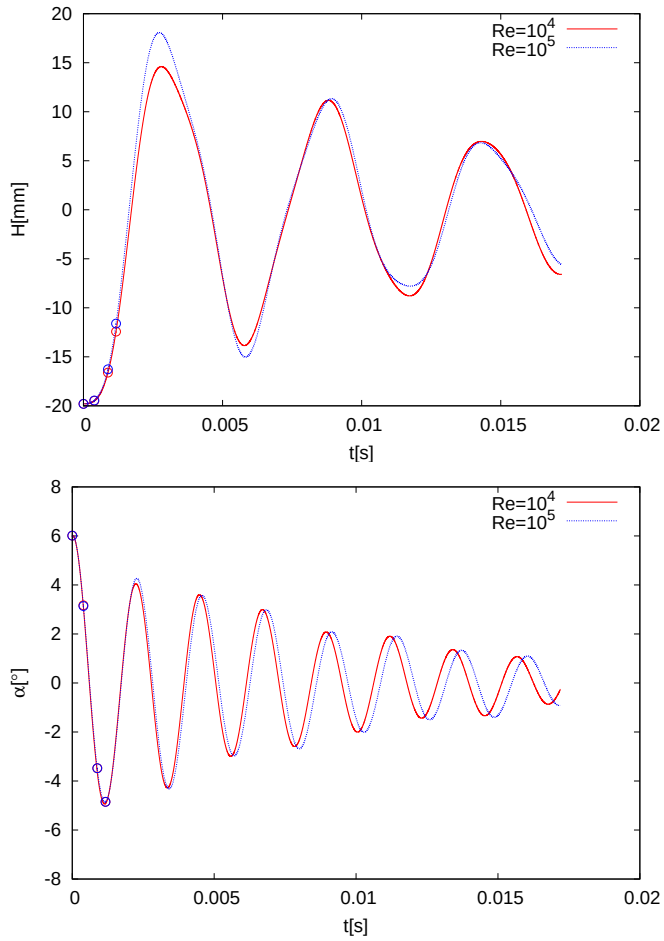

Fig. 7 The graphs of the displacement H and the rotation angle α in dependence on time for far-field velocity 1020 m/s and Mach number $M_\infty = 3.0$.

was released and we continued by the solution of a complete fluid-structure interaction problem.

The initial triangulation (i.e. at time $t = 0$) is shown in Figure 6. In Figure 7, the graphs of the displacement H and the rotation angle $\angle$ in dependence on time are shown for the Reynolds numbers 10^4 and 10^5. Figure 8 shows Mach number distribution in the vicinity of the airfoil at several time instants. One can see well resolved oblique shock wave, shock waves leaving the trailing edge and wake leaving the airfoil.

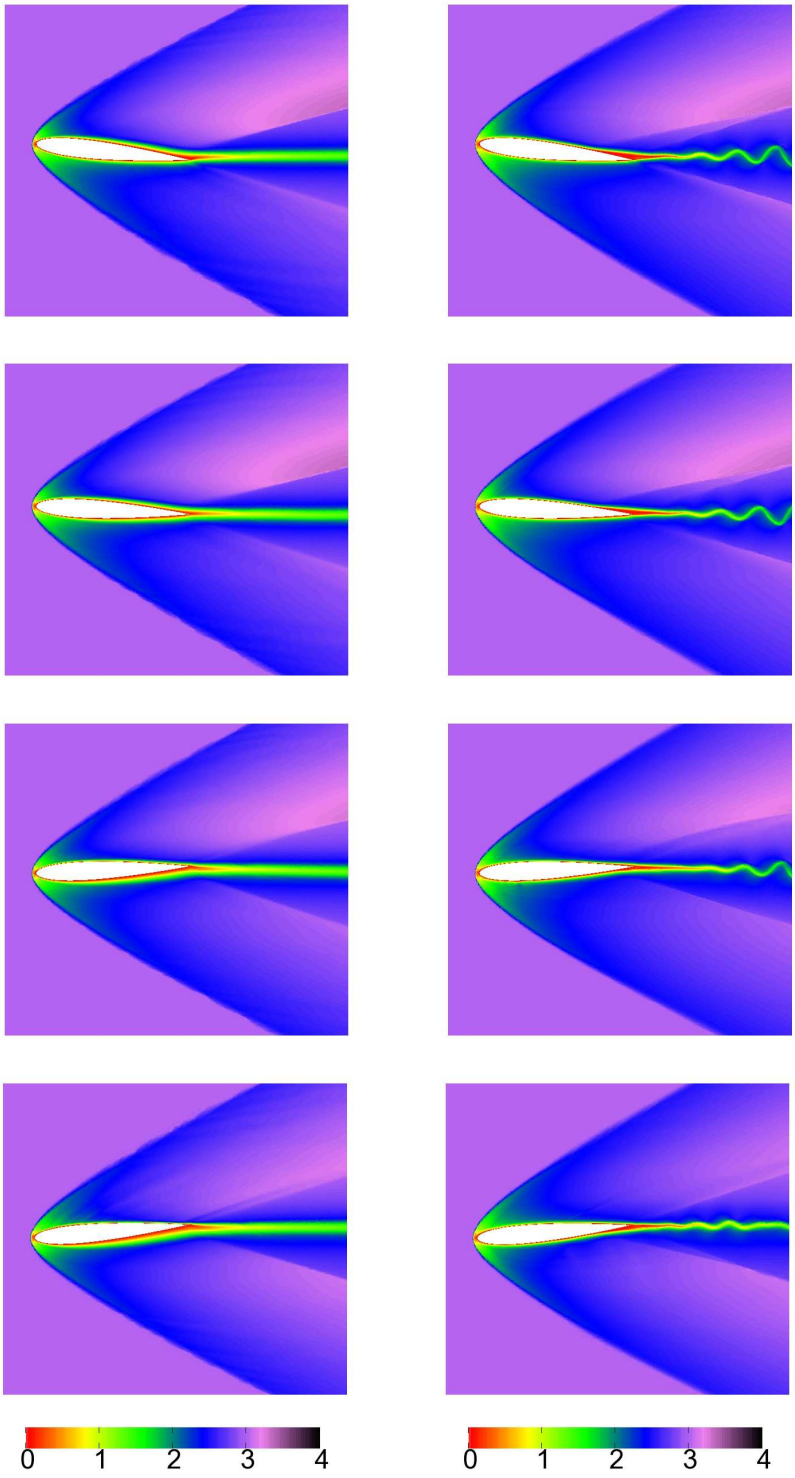

Fig. 8 Mach number distribution at time instants $t = 0.0$ s, 0.00039 s, 0.00078 s, 0.00117 s for the far-field velocity 1020 m/s ($M_\infty = 3.0$) and Reynolds numbers $Re = 10^4$ (left) and $Re = 10^5$ (right).

5 Conclusion

The paper presents a description of a numerical method for the solution of compressible flow in time-dependent domains and the applications to the simulation of airfoil vibrations induced by compressible flow. The gas flow is described by the 2D compressible Navier-Stokes equations in the ALE formulation allowing to take into account time dependence of the computational domain.The flow problem is coupled with the structural problem represented by the system of second-order ordinary differential equations for the vertical displacement and torsional angle of the airfoil. Numerical experiments show that the method is robust with respect to a wide range of Mach numbers and Reynolds numbers. We compare the results of the numerical solution of compressible inviscid flow past an isolated Joukowski airfoil close to incompressible limit with incompressible solution. Further, an example of airfoil vibrations induced by hypersonic viscous flow is presented, demonstrating the applicability of the method to fluid-structure interaction problems with high Mach numbers and Reynolds numbers. The developed technique is based on the following ingredients:
- the ALE method applied to the compressible Navier-Stokes equations,
- the application of the discontinuous Galerkin method to the flow problem discretization,
- semi-implicit linearized time discretization,
- treatment of boundary conditions,
- artificial viscosity applied in the vicinity of internal and boundary layers,
- construction of the ALE mapping and the domain velocity,
- algorithm for the coupling of flow and structural problem.

There are the following subjects for further work:
- realization of further tests of the developed technique,
- solution of problems with large vibrations,
- comparison of obtained results with wind tunnel experiments,
- theoretical analysis of qualitative properties (e.g. stability, convergence) of the numerical methods.

Acknowledgements This research is a part of the grant No. 201/08/0012 of the Czech Science Foundation.

References

1. Bassi, F., Rebay, S.: High-order accurate discontinuous finite element solution of the 2D Euler equations. J. Comput. Phys., **138**, 251–285 (1997).
2. Baumann, C. E., Oden, J. T.: A discontinuous *hp* finite element method for the Euler and Navier-Stokes equations. Int. J. Numer. Methods Fluids, **31**, 79–95 (1999).
3. Bisplinghoff, R. L., Ashley, H., Halfman, R. L.:, Aeroelasticity. Dover, New York (1996).

4. Česenek, J.:, Discontinuous Galerkin method for the solution of compressible viscous flow. Charles University in Prague, Faculty of Mathematics and Physics (2011) (in Czech).
5. Davis, T. A., Duff, I. S.: A combined unifrontal/multifrontal method for unsymmetric sparse matrices. ACM Transactions on Mathematical Software, **25**, 1–19 (1999).
6. Dolejší, V.: Semi-implicit interior penalty discontinuous Galerkin methods for viscous compressible flows. Commun. Comput. Phys., **4**, 231–274 (2008).
7. Dolejší,V., Feistauer, M., Schwab, C.: On some aspects of the discontinuous Galerkin finite element method for conservation laws. Math. Comput. Simul., **61**, 333–346 (2003).
8. Dowell, E. H.: A Modern Course in Aeroelasticity. Kluwer, Dodrecht (1995).
9. Dubcová, L., Feistauer, M., Horáček, J., Sváček, P.: Numerical simulation of interaction between turbulent flow and a vibrating airfoil. Computing and Visualization in Science, **12**, 207–225 (2009).
10. Feistauer, M.: Mathematical Methods in Fluid Dynamics. Longman, Harlow (1993).
11. Feistauer, M., Česenek, J., Horáček, J., Kučera, V., Prokopová, J.:, DGFEM for the numerical solution of compressible flow in time dependent domains and applications to fluid-structure interaction. Proceedings of the 5th European Conference on Computational Fluid Dynamics ECCOMAS CFD 2010, J.C.F. Pereira and A. Sequeira (Eds), Lisbon, Portugal (2010) (published ellectronically), ISBN 978-989-96778-1-4.
12. Feistauer, M., Felcman, J., Straškraba, I.: Mathematical and Computational Methods for Compressible Flow. Clarendon Press, Oxford (2003).
13. Feistauer, M., Horáček, J., Kučera, V., J. Prokopová, J.:, On numerical solution of compressible flow in time-dependent domains. Mathematica Bohemica, **137**, 1–16 (2012).
14. Feistauer, M., Kučera, V.: On a robust discontinuous Galerkin technique for the solution of compressible flow. J. Comput. Phys., **224**, 208–221 (2007).
15. Naudasher, E., Rockwell, D.: Flow-Induced Vibrations. A.A. Balkema, Rotterdam (1994).
16. Nomura, T., Hughes, T. J. R.: An arbitrary Lagrangian-Eulerian finite element method for interaction of fluid and a rigid body. Comput. Methods Appl. Mech. Engrg., **95**, 115-138 (1992).
17. Sváček, P., Feistauer, M., Horáček, J.: Numerical simulation of flow induced airfoil vibrations with large amplitudes. J. of Fluids and Structures, **23**, 391-411 (2007).
18. van der Vegt, J. J. W., van der Ven, H.: Space-time discontinuous Galerkin finite element method with dynamic grid motion for inviscid compressible flow. J. Comput. Phys., **182**, 546–585 (2002).
19. Vijayasundaram, G.: Transonic flow simulation using upstream centered scheme of Godunov type in finite elements. J. Comput. Phys., **63**, 416–433 (1986).